Direct measurement of cortical force generation and polarization in a living parasite

Rachel V. Stadler[a], Lauren A. White[a], Ke Hu[b], Brian P. Helmke[a], and William H. Guilford[a,*]
[a]Department of Biomedical Engineering, University of Virginia, Charlottesville, VA 22908; [b]Department of Biology, Indiana University, Bloomington, IN 47405

ABSTRACT **Apicomplexa is a large phylum of intracellular parasites that are notable for the diseases they cause, including toxoplasmosis, malaria, and cryptosporidiosis. A conserved motile system is critical to their life cycles and drives directional gliding motility between cells, as well as invasion of and egress from host cells. However, our understanding of this system is limited by a lack of measurements of the forces driving parasite motion. We used a laser trap to measure the function of the motility apparatus of living *Toxoplasma gondii* by adhering a microsphere to the surface of an immobilized parasite. Motion of the microsphere reflected underlying forces exerted by the motile apparatus. We found that force generated at the parasite surface begins with no preferential directionality but becomes directed toward the rear of the cell after a period of time. The transition from nondirectional to directional force generation occurs on spatial intervals consistent with the lateral periodicity of structures associated with the membrane pellicle and is influenced by the kinetics of actin filament polymerization and cytoplasmic calcium. A lysine methyltransferase regulates both the magnitude and polarization of the force. Our work provides a novel means to dissect the motile mechanisms of these pathogens.**

Monitoring Editor
Thomas D. Pollard
Yale University

Received: Jul 18, 2016
Revised: Jan 19, 2017
Accepted: Feb 10, 2017

INTRODUCTION

Toxoplasma gondii (*Toxoplasma*) is an obligate, intracellular, protozoan parasite that causes the zoonotic disease toxoplasmosis. Although estimates of seroprevalence vary widely among different countries and cultures, it is prevalent almost worldwide (Pappas *et al.*, 2009). Humans are most commonly infected through the consumption of tissue cysts in undercooked meat or of oocytes shed by infected felines (Tenter *et al.*, 2000; Kijlstra and Jongert, 2008). The disease is particularly dangerous for pregnant women and immunocompromised individuals, leading to spontaneous abortions, transmission of congenital toxoplasmosis from mother to child, and cases of encephalitis (Tenter *et al.*, 2000). *Toxoplasma* is also a model organism for understanding parasites in the large and closely related Apicomplexa phylum that includes the causative organisms of several disruptive diseases, including *Theileria*, *Cryptosporidium*, and *Plasmodium* genera. *Plasmodium* is the causative agent of malaria, which is responsible for ~660,000 mortalities annually and significant morbidity (World Health Organization, 2012). *Toxoplasma*, *Theileria*, and *Eimeria* are particularly notable for their effects on livestock (Burney and Lugton, 2009; Dubey, 2009; Fornace *et al.*, 2013).

Unlike many other parasitic organisms, the apicomplexans do not depend on host-mediated routes (e.g., phagocytosis) for entry (Sibley and Andrews, 2000); the actin cytoskeleton of the host cell appears to play only a minor role (Gonzalez *et al.*, 2009). In *Toxoplasma*, entry into host cell is an active process driven by the actomyosin complex of the parasites themselves. These protozoa have clear polarity, with anterior (apical) and posterior (basal) ends with highly organized cytoskeletal complexes (Nichols and Chiappino, 1987; Hu *et al.*, 2006; Figure 1). The apical end of the protozoan secretes adhesive proteins such as micronemal adhesion protein 2 (MIC2) from membrane-bound organelles (micronemes; Carruthers *et al.*, 1999). These serve as host-binding receptors. On the cytoplasmic face of the plasma membrane (Figure 1C), the adhesins are believed to bind indirectly to actin filaments (Soldati and Meissner, 2004). These actin filaments are engaged by a class XIV myosin (MyoA)—a small, single-headed, fast myosin unique to the phylum

This article was published online ahead of print in MBoC in Press (http://www.molbiolcell.org/cgi/doi/10.1091/mbc.E16-07-0518) on February 16, 2017.

*Address correspondence to: William Guilford (guilford@virginia.edu).

Abbreviations used: AKMT, apical complex lysine methyltransferase; CytoD, cytochalasin D; IMC, inner membrane complex; Jas, jasplakinolide; MIC2, micronemal adhesion protein 2.

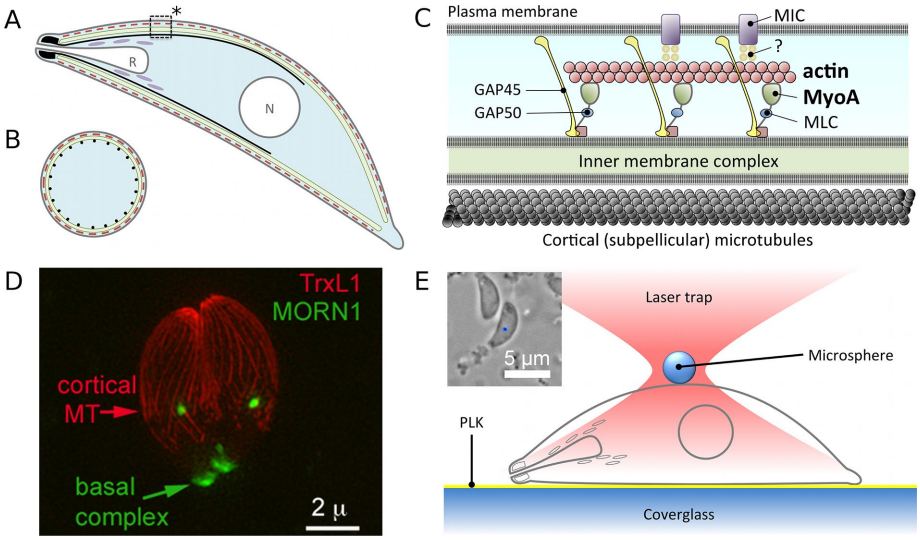

FIGURE 1: The motile apparatus of *T. gondii* and our experimental model. Schematic diagrams of *Toxoplasma* are shown in (A) longitudinal cross-section and (B) transverse cross-section, including the plasma membrane (gray), rhopteries (R), and nucleus (N). The apex (left) includes a tubulin-rich structure from which there extends an array of 22 cortical (subpellicular) microtubules (black). These underlie the inner membrane complex (green). The glideosomes (dashed red) lie between the inner membrane complex and the plasma membrane. The boxed area (asterisk) is expanded in C to illustrate more clearly the glideosomes. (D) The fluorescence image shows the organization of the cortical microtubules in a pair of *T. gondii* labeled by mEmeraldFP-TrxL1 (pseudocolored red), a microtubule-associated protein. The basal complex is labeled by mTagRFP-TgMORN (pseudocolored green; Liu *et al.*, 2016). (E) In our experiments, we coat a coverglass with poly-L-lysine (PLK), to which we subsequently adhere parasites (gray outline). A laser trap (red) is used to capture a microsphere and bring it into contact with the upper surface of the parasite. The relative scales of parasite and microsphere are approximately correct in this illustration. Inset, a bright-field micrograph of a trapped microsphere (blue) bound to a live parasite. This image combines two focal planes in order to make both the microsphere and the parasite appear in focus.

(Herm-Gotz *et al.*, 2002; Meissner *et al.*, 2002; Baum *et al.*, 2006; Heaslip *et al.*, 2010; Andenmatten *et al.*, 2013). Two gliding-associated proteins (GAP45 and GAP50) anchor MyoA to the pellicle (Gaskins *et al.*, 2004), also known as the inner membrane complex (IMC; Wong and Desser, 1976; Morrissette *et al.*, 1997), which consists of two layers of membrane closely juxtaposed and located just underneath the plasma membrane. This structure, spanning from the plasma membrane to the IMC, is commonly known as a glideosome. Both motility and invasion of MyoA knockout and knockdown mutants are severely impaired, consistent with it being the major motor for driving motility (Meissner *et al.*, 2002; Andenmatten *et al.*, 2013).

The current model for gliding proposes that the myosin motor is fixed in place on the IMC and that pulls actin filaments toward the basal end of the cell (Opitz and Soldati, 2002). In turn, via adaptor proteins, the actin filaments pull on MIC2 molecules, which bridge the plasma membrane to bind to host cells. Thus forward motion of the parasite relative to host cells is driven by rearward transport of actin filaments and their bound adhesins relative to the parasite body. Meanwhile, MICs are secreted from the apical pole of the cell to form new adhesions, while old adhesions are cleaved by proteases at the basal end of the parasite.

Although this model is an attractive hypothesis, the direction and magnitude of forces generated at the cell surface have never been directly or accurately measured. Münter *et al.* (2009) measured the tension generated in the substrate below adherent, motile *Plasmodium berghei* sporozoites by traction force microscopy. This yields a measure of the force per unit area across the surface of the parasite rather than an absolute directional force measured at a single point on the parasite. Further, the technique has limited temporal and spatial resolution. A more recent study showed that *Plasmodium* sporozoites could pull surface-adherent microspheres free of an optical trap (Quadt *et al.*, 2016), showing that motile forces are indeed generated at the plasma membrane. However, this approach (escape force) provides neither directional data nor an accurate, time-dependent measure of force. Thus it is still not known how whole-cell movement is related to the activity of the motor complex or how the activity of this complex is regulated. Direct measurements of the activity of the motor complex are needed to understand the biomechanics of motility and invasion of *Toxoplasma* and of apicomplexans in general.

Here we develop a novel experimental system that uses a laser trap to measure localized intracellular force generation in living parasites via external attachments to transmembrane adhesion receptors. The *Toxoplasma* host-binding receptors serve as a direct mechanical linkage to the glideosome complex inside the cell, affording the opportunity to interact directly and mechanically with a nonmuscle actomyosin system. Furthermore, *Toxoplasma* provides a unique opportunity for directly measuring force generation at the membrane cortex with a precision not possible in animal cells. Its motility apparatus contains <10 known components (likely to account for the majority of the key components), compared with the massive, >200-component focal adhesion complex of mammalian cells. Furthermore, the actomyosin complex at the cortex is spatially segregated from microtubule cytoskeleton by the IMC, greatly simplifying the interpretation of the data.

RESULTS

We based our experimental protocol on previous work measuring generation of force by kinesin and dynein in the flagella of living *Chlamydomonas*, an alga (Laib *et al.*, 2009). First, flow cells were prepared by separating two stacked coverslips with Mylar shims, coated with poly-L-lysine to adhere parasites to the surface, and loaded with *Toxoplasma*. After a 20-min incubation, a suspension was loaded of 0.6-μm microspheres coated with serum proteins in culture medium. The laser trap was used to capture a microsphere from suspension and place it on the surface of the immobilized parasite (Figure 1, E and inset). The microsphere bound to the cell surface immediately, as shown by our inability to forcibly remove the microsphere from the cell surface using the laser trap once it had been in contact. Thus any subsequent displacement of the microsphere across the surface of the membrane reflected the cortical forces. The motile behaviors of the microsphere were observed under both "unconstrained" (laser trap off) and "constrained" (laser trap on) conditions at room temperature (~24°C), a temperature at which *Toxoplasma* remains invasive (Nichols and O'Connor, 1981).

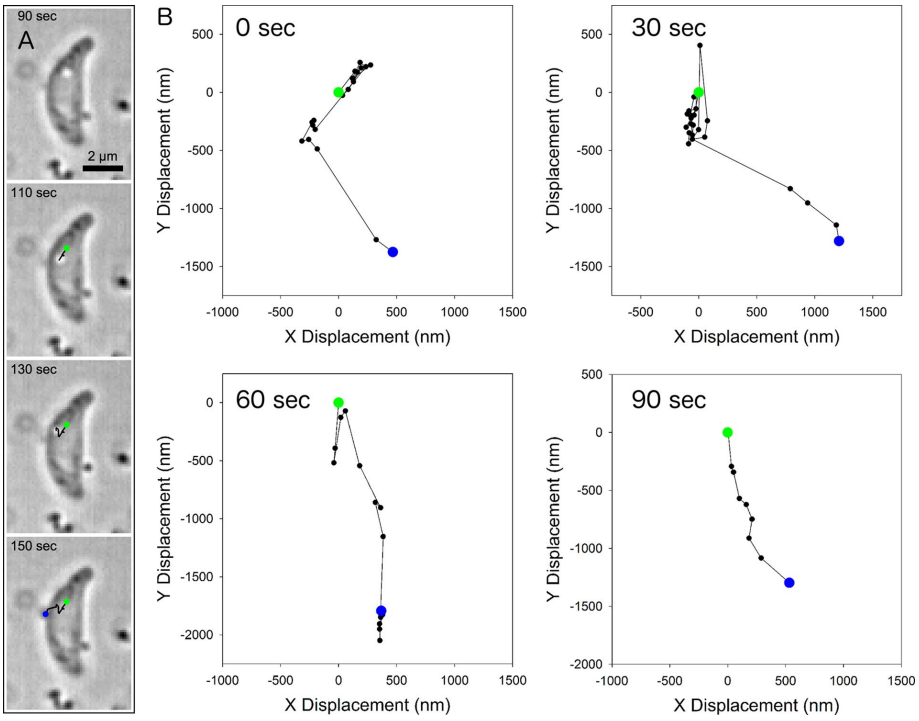

FIGURE 2: Unconstrained microspheres are transported rearwards from apical to basal across *T. gondii*, but only after a delay. (A) Microspheres were deposited (green arrow) on and bound to parasites near their apical poles using a laser trap and subsequently released after being constrained for a set period of time. (B) The motion of the microsphere was tracked every 5 s using cross-correlation of video frames from the moment of release (green data point) to the moment the microsphere touched the substrate at the edge of the cell (blue data point). The exemplar in A was released after 90 s of being constrained by the laser trap, and the time stamps in each frame indicate the time from when the microsphere first made contact with the cell. (B) Example tracking plots of microspheres released after being constrained by the trap for 0, 30, 60, or 90 s. Microspheres were transported roughly toward the basal pole of the cell, which in these graphs is always downward (negative in *y*), although typically also with significant lateral movements. When the microsphere was released immediately after being deposited, initial random motion of the microsphere was followed at ~50 s by sudden lateral jump and subsequently rearward transport (see 0 s). In contrast, rearward transport was almost immediate when the microsphere was released 60 or 90 s after it was deposited.

Membrane-bound microspheres display on- and off-axis movements when unconstrained

The gliding model of motility suggests that substrates attached to the surface of *Toxoplasma* should be "capped"—that is, objects or molecules cross-linked to cell surface proteins should be moved toward the basal end of the cell. Capping of antibodies has been reported in *Eimeria* (Russell and Sinden, 1981; Speer *et al*., 1985), *Plasmodium* (Stewart and Vanderberg, 1991), *Gregarina* (Russell, 1983), and *Toxoplasma* (Dzbenski *et al*., 1976) but only as snapshots of parasites fixed at various time points during invasion or motility. Capping of microspheres has been reported in living *Gregarina*, in which freely moving parasites transport concanavalin A–coated microspheres rearward at a velocity similar to that of forward motion of the parasite (King, 1981).

To measure capping in *Toxoplasma* in real time, we used the laser trap to place microspheres on adherent parasites. As mentioned, microspheres bound immediately to the parasite. We then turned off the laser trap at one of four time points (0, 30, 60, or 90 s), leaving them unconstrained by the laser trap and free to be moved by the cell. We captured bright-field images every 5 s thereafter and determined the position of the microsphere using cross-correlation (Cheezum *et al*., 2001; Figure 2A). We found that the motion of the deposited microspheres displayed time-dependent polarization. If the microsphere was released immediately after deposition (0 s), then a period of random motion on the cell surface was followed after 55 ± 3 s by a lateral jump of 261 ± 53 nm, roughly perpendicular to the long axis of the cell. The microsphere was subsequently transported toward the basal end at an average velocity of 30 ± 4 nm/s (148 ± 18 nm/s maximum, $n = 9$; Figure 2, 0 s) at room temperature (~24°C). The large difference between the average and maximum velocities resulted from frequent pauses and reversals of the microsphere during rearward transport.

The fact that microspheres were not immediately and directly pulled toward the basal end of the cell suggests that the motile system of these organisms is either not preactivated or not preassembled with established directionality. Instead, a chain of events is necessary for glideosomes to activate and/or their directional activity to orient toward the basal end of the cell. Indeed, if instead we constrained the microsphere with the laser trap for 30 s and then released it, the period of random motion was shortened by 30 s (Figure 2, 30 s). If the microsphere was held for 60–90 s and then released, it was immediately transported toward the basal end at an average of 28 ± 4 nm/s (210 nm/s maximum, $n = 5$; Figure 2, 60 and 90 s and A). Note that the rearward transport of the microspheres was always sufficiently off-axis that they collided with the substrate before reaching the basal pole of the cell. This may suggest a helical path across the three-dimensional (3D) surface of the cell, such as the one set by the cortical microtubules that twist helically around the parasite (Figure 1D).

Force generation by *Toxoplasma* is not prepolarized but instead becomes polarized

The general features of random motion, lateral displacement, and polarized motion we observed under the unconstrained conditions were also observed when the microsphere was constrained by the laser trap. When held continuously in the laser trap, microspheres typically underwent an initial period of randomly directed motion with only a modest rearward bias. We refer to this as the apolar phase. The force generation eventually aligned to the long axis of the cell and became directed toward the basal end (Figure 3, A and B)—the polar phase. The elapsed time was 59 ± 7 s ($n = 19$) from when the trapped microsphere bound to the surface of the parasite to when the cell transitioned from apolar to polar force generation. This time lag was similar to what we observed in unconstrained (trap off) conditions. Analysis of the two-dimensional (2D) displacement during the initial apolar period showed that these motions were not due to Brownian motion; their magnitudes were significantly greater than when the microsphere was held in the laser trap before cell contact and higher than one would predict based on the stiffness of

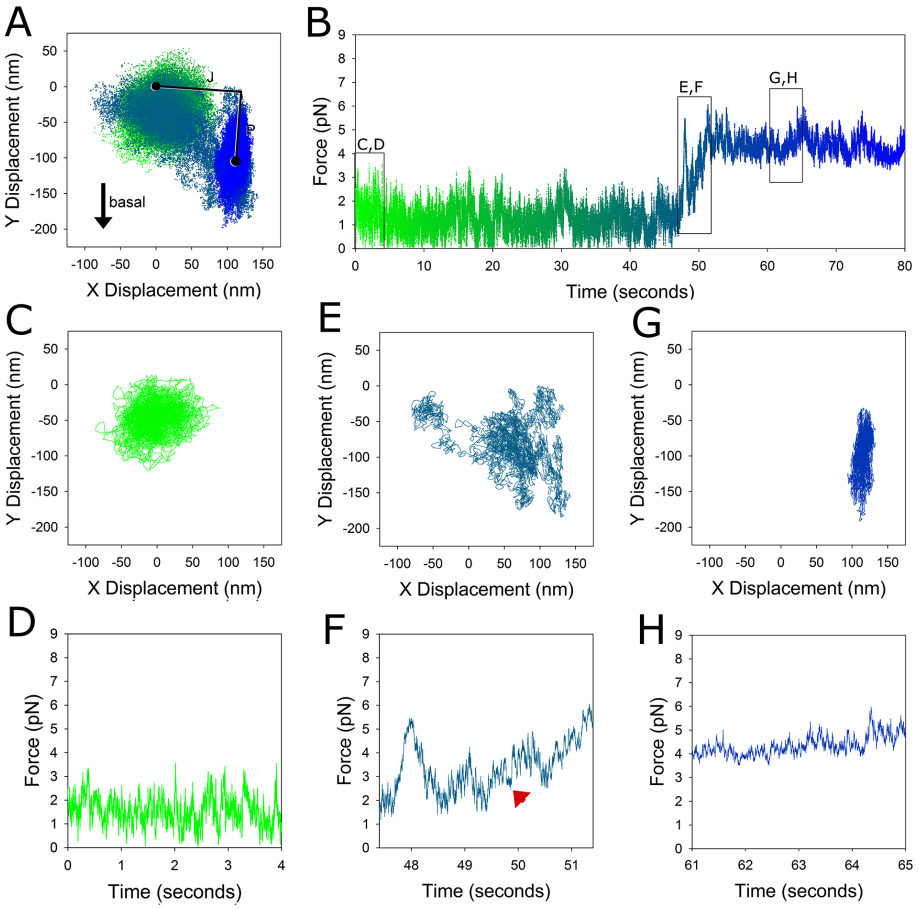

FIGURE 3: Force generation by *Toxoplasma* is not prepolarized but instead becomes polarized. (A, B) The 2D plots of microsphere displacement (A) and corresponding temporal plot of force generation (B) by the parasite measured in the laser trap under control conditions. Note that a segment of high noise and without directional preference (green) is followed after tens of seconds by directional motion of the microsphere (cyan-blue)—the apolar and polar phases, respectively. The basal end of the parasite is toward the bottom of each 2D plot (arrow, negative in *y*). A lateral displacement or "jump" (*J*) typically occurs at transition between the apolar and polar phases. Subsequently a polar force (*P*) is generated along the long axis of the parasite. Magnifications of the apolar, transitional, and polar phases are shown as 2D displacement plots (C, E, G) and temporal plots (D, F, H). The red arrow indicates a discrete pause or step in motion. In each graph, the data are color coded by time, from green, representing 0 s, to blue, representing 80 s.

the laser trap and the diameter of the microsphere (~15 nm root mean square [RMS]).

Of importance, the constrained condition allows us to measure displacement of the microsphere with nanometer spatial resolution and a bandwidth limited only by viscous drag on the microsphere. It also allows us to calculate the cortical force because the laser trap registers changes in the microsphere's displacement, and displacement is proportional to force. The laser trap is calibrated before every measurement to determine the trap stiffness, which sets the relationship between the measured displacement and force (0.02 pN/nm typical).

Mean force generated during the apolar phase (1.9 ± 0.2 pN) was significantly less than during the polar phase ($p < 0.001$; Figure 3, B, D, and H, and Table 1). However, the variation in force during the apolar phase was large enough that the *maximum* absolute force (3.8 ± 0.3 pN) during the apolar phase was nearly as high as the *mean* absolute force during the polar phase (4.6 ± 0.5; $p = 0.17$). This similarity reflected the fact that there was tremendous variance in force during the apolar phase and less variance during the polar phase: 1.1 ± 0.6 versus 0.6 ± 0.4 pN^2, respectively. The 4.6 pN measured in the polar phase was a stall force, meaning that the motor-driven polar motion of the microsphere was stopped by the laser trap. We know that it was a stall because the microsphere progressed toward the basal end of the cell when we released it from the laser trap (see previous section and Figure 2).

These behaviors were not an artifact of parasite heating by the laser trap. We tested this by directing an empty laser trap at a parasite for 180 s. We subsequently captured a microsphere and performed an experiment as described previously on the same parasite. The mean absolute force generated during the apolar (1.7 ± 0.3 pN) and polar phases (4.1 ± 0.5 pN) did not differ significantly between these and the previous experiments ($n = 6$, $p = 0.3$).

The forces given were magnitudes—the difference between the force at the prescribed time and that measured at baseline (the first 50 ms after binding of the microsphere to the parasite). It is independent of direction. However, because force generation becomes polarized, we can also measure a "main-axis" force component during the polar phase—the component of force that is parallel to the main force-generating axis once it becomes polarized. We did this by fitting a line through the final 20 s of 2D force data (*P* in Figure 3A) and finding the mean of those data parallel to the line (see *Materials and Methods* for details). In wild-type cells, the main-axis force was 3.3 ± 0.9 pN ($n = 19$; Table 1). This was predictably less than the 4.6-pN absolute force measured from the origin because some of the latter force was directed laterally. Both parameters have value because forces off-axis with respect to cytoskeletal tracks can affect motor function (Block *et al.*, 2003), and the main-axis force will presumably drive the forward motion of the cell.

The main-axis force component was predominantly aligned with the long axis of the parasite; the average of the angle differences between the main-axis force component and the long axis of the parasite was 35 ± 8°. In addition, we calculated the anisotropy (*r*), or the directional dependence, of force along this line as a measure of the *extent* to which the force is directed along a single axis. An anisotropy value of 0 indicates absolutely no directional bias, whereas a value of 1 indicates that all of the force is directed along the main axis. In practice, anisotropy increased from 0.13 ± 0.03 during the apolar phase to 0.67 ± 0.01 during the polar phase. All of these data are listed in Table 1.

Note that even during the apolar phase, there was *some* directional bias in the generation of force, even if anisotropy measurements show that force generation to be ill aligned. For example, in Figure 3, the green clustered data points representing the apolar phase are not centered on the baseline. The 1.9-pN mean force

Time (s)	Measured parameter	Wild-type parasites					AKMT KO			AKMT KO–complement
		Untreated (n = 19)	Iono 1 µM (n = 16)	CytoD 200 nM (n = 5)	CytoD 1 µM (n = 4)	Jas 2 µM (n = 12)	Untreated (n = 6)	Iono 1 µM (n = 5)	Jas 2 µM (n = 6)	Untreated (n = 5)
0–10	Mean absolute force (pN)	1.9 ± 0.2	3.7 ± 0.3	1.2 ± 0.2	0.5 ± 0.1	4.0 ± 0.3	1.3 ± 0.2	1.1 ± 0.2	2.5 ± 0.5	1.8 ± 0.3
0–30	Maximum absolute force (pN)	3.8 ± 0.3	6.9 ± 0.5	3.0 ± 0.4	1.4 ± 0.3	6.4 ± 0.6	2.7 ± 0.4	3.5 ± 0.7	6.0 ± 0.5	3.3 ± 0.8
0–10	Mean anisotropy	0.13 ± 0.03	0.60 ± 0.02	0.12 ± 0.03	0.11 ± 0.02	0.09 ± 0.02	0.17 ± 0.02	0.57 ± 0.01	0.14 ± 0.02	0.12 ± 0.05
70–80	Mean absolute force (pN)	4.6 ± 0.6	4.8 ± 0.6	2.8 ± 0.2	0.6 ± 0.2	3.7 ± 0.3	1.6 ± 0.3	2.1 ± 0.5	3.5 ± 0.6	4.1 ± 0.5
60–80	Maximum absolute force (pN)	6.0 ± 0.9	7.1 ± 0.8	4.6 ± 0.5	1.5 ± 0.4	6.6 ± 0.7	2.6 ± 0.3	4.7 ± 0.8	6.1 ± 0.3	5.2 ± 0.5
70–80	Main-axis force magnitude (pN)	3.3 ± 0.9	2.4 ± 0.5	1.3 ± 0.3	0.5 ± 0.3	1.4 ± 0.9	1.0 ± 0.3	1.7 ± 0.3	1.7 ± 0.3	2.1 ± 0.3
70–80	Mean anisotropy	0.67 ± 0.01	0.61 ± 0.03	0.10 ± 0.03	0.12 ± 0.04	0.12 ± 0.04	0.17 ± 0.03	0.57 ± 0.01	0.12 ± 0.03	0.59 ± 0.04
70–80	Mean lateral displacement (nm)	139 ± 20	39 ± 8	N/A	N/A	N/A	N/A	30 ± 6	N/A	148 ± 13

Errors are provided as SEM. N/A, jump distance not shown because the movement of the microsphere does not have a dominant axis (i.e., low anisotropy) under these conditions.

TABLE 1: Parameters derived from the data for most of the experimental conditions described in this article.

during the apolar phase was directed toward the basal end of the parasite.

The measurements described to this point were taken midway between the apical and basal ends of the parasite. To determine whether there is a difference in the development of the cortical force at different points along the longitudinal axis of the parasite, we trapped two 0.6-µm microspheres simultaneously 4.0 µm apart and deposited them simultaneously ~0.5 µm from their respective ends of the parasite. The maximum force during the initial period, the final stall force, and the orientation of the force vector (apical → basal) were not different at the apical from at the basal end of the parasite, indicating that there is no intrinsic difference in the force-generating apparatus in these two regions. However, there was a significant (p = 0.02) delay in the transition from apolar to polar force generation at the basal end compared with the apical end (Supplemental Figure S1). This delay of 3.4 ± 0.8 s was small compared with the delay of 69 ± 6 s between microsphere binding to the cell surface and the polar orientation of the force (n = 13). This lag suggests either a relay system propagating from the apical to the basal end of the parasite or local differences in the signaling that regulate the functionality of the underlying motility apparatus.

Occasional discrete pauses or steps are observed, particularly during the apolar phase and the transition to the polar phase (Figure 3F and Supplemental Figure S2). However, this in vivo system is inherently noisy. The baselines associated with individual steps tended to drift relative to one another over time, and we were therefore unable to establish a consistent step size.

The transition between apolar and polar motility suggests a constraint imposed on the glideosome by the underlying pellicle structure

We observed that when parasites transition from apolar to polar motility, there is often an abrupt jump in lateral displacement under both unconstrained (Figure 2) and constrained (Figure 3A) conditions. This manifested in a 2D plot as the main-axis force vector not passing through the zero-displacement baseline established when the microsphere first became bound to the parasite. We analyzed these data by calculating a line that passes through the baseline and that also is perpendicular to the main-axis force vector. The distance from the origin to the intersection between those lines is the jump distance (J in Figure 3A).

The mean absolute distance jumped was 139 ± 20 nm (n = 19) but ranged from 56 to 223 nm. The variation in jump distance that we measure in different experiments might be explained by the fact that our deposition of the microsphere onto the surface of the parasite is random with respect to any underlying structure. Because the jumps are symmetrical (occurring to the left or right of the main-axis force vector), this implies the existence of underlying "tracks" for polar motility that lie ~278 ± 40 nm apart.

Microtubules underlie the inner membrane complex of Apicomplexa (Figure 1, A and B). These cortical (subpellicular) microtubules number 22 (Nichols and Chiappino, 1987) and are evenly spaced around *Toxoplasma*'s circumference of ~6.3 µm (estimated from a midplane width of ~2 µm). They are thus spaced at ~286 nm—similar to the spacing we inferred from the jumps in lateral displacement. These data raise the intriguing possibility that the motor system associated with the plasma membrane might be organized along the cortical microtubules or other structures within the pellicle (Wong and Desser, 1976; Morrissette *et al.*, 1997), thus conferring the long-range directionality of parasite movement.

Increased intracellular calcium hastens the apolar-to-polar transition

Rapid fluxes in intracellular [Ca^{2+}] have been suggested as a key regulatory step for motility activity in *Toxoplasma* (Wetzel *et al.*, 2004). Calcium ionophores induce micronemal protein release (Carruthers and Sibley, 1999) and conoid extrusion (Monteiro *et al.*, 2001) and induce the early egress of *Toxoplasma* parasites from host cells (Caldas *et al.*, 2007, 2010).

To determine whether [Ca^{2+}] influences the magnitude, directionality, or onset of force generated by glideosomes, we treated parasites with 1 µM ionomycin, a calcium ionophore ($n = 16$). Compared to untreated cells, treatment with ionomycin resulted in a slightly greater mean force during the polar phase than with controls—4.8 ± 0.6 versus 4.6 ± 0.6 pN—although this difference was not significant ($p = 0.4$; Table 1). However, 88% of ionophore-treated parasites displaced the microsphere immediately after it was placed on the cell surface, with no observable apolar period (Figure 4). The lateral jump distance was small (39 ± 8 nm); it is likely that the jump that that precedes the polar phase had completed before we could make the measurement. Another possibility is that calcium influx induced by ionomycin eliminates the need to align with a preassembled track. Either way, these data show that calcium signaling plays a crucial role in initiating and/or maintaining the polar phase.

Inhibition of polymerization of actin reduces force and abrogates polarity

Because the actomyosin complex is the only known cytoskeletal structure located between the plasma membrane and the inner membrane complex, the cortical force we observed is likely exerted by myosin on actin through the transmembrane adhesive proteins (such as MIC2s). Further, regulation of the kinetics of actin polymerization is vital to parasite motility. Inhibition of actin polymerization blocks motility (Dobrowolski and Sibley, 1996); induction of longer, stabilized actins in *Toxoplasma* leads to aberrant and unproductive gliding (Wetzel *et al.*, 2003).

To determine whether the forces and displacements measured here depend on actomyosin activity, we treated parasites with 200 nM cytochalasin D (CytoD) to inhibit actin polymerization. We found that parasites did not polarize ($r = 0.10 \pm 0.03$) and generated reduced forces compared with control after 80 s of parasite contact—2.8 ± 0.2 pN ($n = 6$). This is consistent with previous work showing that parasite motility is inhibited in the presence of 200 nM cytochalasin D (Dobrowolski and Sibley, 1996) and indicates that this level of nondirectional cortical force cannot generate significant parasite movement. Cytochalasin D treatment at 1 µM further reduced the mean and maximum absolute forces during the apolar phase to 0.5 ± 0.1 and 1.4 ± 0.3 pN, respectively ($n = 4$; Figure 5, A and B), and these did not increase over time ($p = 0.2$; Table 1).

Unregulated polymerization of actin initially increases force but abrogates polarity

The actin filament stabilizer jasplakinolide (Jas) has been shown to inhibit motility and invasion by Apicomplexa (Shaw and Tilney, 1999; Wetzel *et al.*, 2003; Skillman *et al.*, 2011). Further, treatment with Jas lengthened actin filaments in *Toxoplasma* from 100 to 240 nm (Sahoo *et al.*, 2006). We treated parasites with Jas to determine whether short actin filaments specifically, and actin filament dynamics generally, are important to direction finding in *Toxoplasma*.

Parasites treated with 2 µM Jas ($n = 11$) did not exhibit the characteristic transition to a sustained force as seen in control parasites; in fact, they seldom showed a significant *net* displacement but instead generated large displacements of the microsphere in random directions. The associated large but highly variable apolar forces were generated from the moment of microsphere binding to the parasite (Figure 5, C and D). The mean forces observed in Jas-treated parasites were larger than for controls during their apolar phase—4.0 ± 0.3 versus 1.9 ± 0.2 pN, respectively ($p < 0.001$)—but were similar to the forces generated during the polar phase of control cells ($p = 0.19$). Further, the average maximum displacement under these conditions was 239 ± 28 nm, similar both to the length measured previously of Jas-treated actin filaments in parasites (Sahoo *et al.*, 2006) and to twice the jump distance measured in untreated cells.

These data are consistent with video microscopy studies that showed a substantial increase in velocity for *Toxoplasma* treated with Jas but also showed frustrated motility due to frequent changes in direction (Wetzel *et al.*, 2003). We hypothesize that in the presence of Jas, actin filaments grow too long and too quickly and are either unable to orient to the long axis of the parasite or are not subject to preferential polymerization along the correct axis, resulting in mixed polarity. It is also interesting that the maximum force for untreated and JAS-treated parasites is similar (6.0 vs. 6.6 pN, $p = 0.5$; Figure 6), which suggests a fundamental limit on the maximum force. Candidate mechanisms for a maximum force include an absolute limit on the length to which actin filaments may grow in these parasites, and a limit on the number of myosin motors accessible to any given filament.

Force measurements show that a novel lysine methyltransferase might be involved in regulating actin polymerization

The novel lysine methyltransferase AKMT is an important regulator of motility in *Toxoplasma* (Heaslip *et al.*, 2011). The loss of AKMT causes major defects in calcium-sensitive parasite motility activation, resulting in a dramatic delay in parasite dispersion during egress and ~10-fold decrease in invasion efficiency but with no reduction in microneme secretion upon treatment with calcium ionophore. We used our laser trap assay with AKMT-knockout parasites to position this enzyme within the regulatory pathway for motility.

In AKMT-knockout parasites, the alignment of force to the long axis of the cell was slow, force development did not become fully directional ($r = 0.17 \pm 0.03$), and

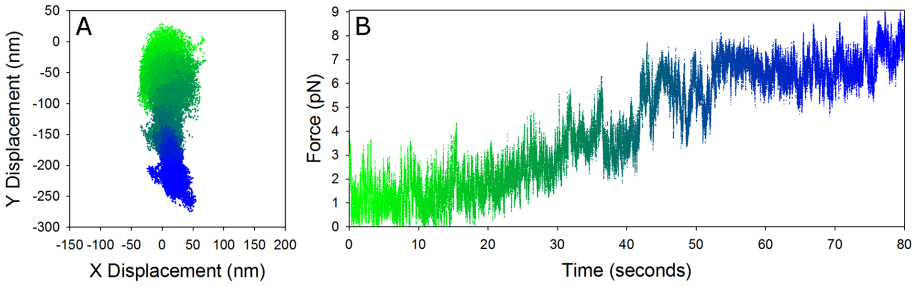

FIGURE 4: An increase in intracellular calcium concentration causes a transition from apolar to polar generation of force. A 2D plot of displacement (A) and corresponding temporal plot of force magnitude (B) of a wild-type cell treated with the Ca^{2+} ionophore ionomycin (1 µM). In each graph, the data are color coded by time, from green, representing 0 s, to blue, representing 80 s. The basal end of the parasite is toward the bottom of the 2D plot (negative in *y*).

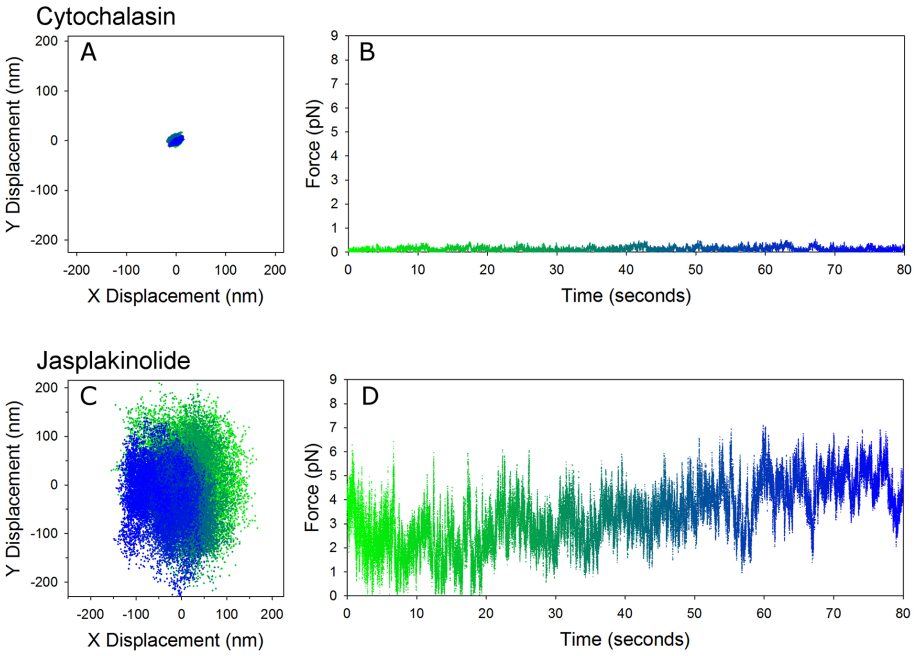

FIGURE 5: Both the magnitude and directionality of the cortical force are affected by the kinetics of actin polymerization. (A, B) A 2D plot for microsphere displacement (A) and corresponding temporal plot of force generation (B) for a microsphere bound to a parasite treated with 1 μM cytochalasin D, showing that disassembling actin filaments markedly reduces force and motion of the microsphere and abrogates the transition to polar motion. (C, D) A 2D plot for microsphere displacement (C) and corresponding temporal plot of force generation (D) for a microsphere bound to a parasite treated with 2 μM Jas, showing that stabilizing actin filament generates large but highly variable apolar forces from the moment of microsphere contact but abrogates the transition to polar force. In each graph, the data are color coded by time, from green, representing 0 s, to blue, representing 80 s. The basal end of the parasite is toward the bottom of each 2D plot (negative in *y*).

directional excursions were small when compared with wild-type cells (Figure 7). Further, the mean force developed by these mutants was low: 1.6 ± 0.3 pN (Figure 7, KO; $n = 6$). Knockout parasites complemented with a FLAG-tagged AKMT gene (KO-Comp; Heaslip *et al.*, 2011) show complete recovery of function to control levels; they polarized ($r = 0.59 \pm 0.04$), underwent a lateral jump of similar magnitude (148 ± 13 nm) to control, and generated nearly identical forces as control cells during their apolar and polar phases ($n = 5$, $p = 0.6$; Figure 7 and Table 1).

The low stall force in the AKMT-knockout parasites could be caused by a defect in force transmission from the intracellular motor complex through the membrane or a defect in the force generation itself. To distinguish these two possibilities, we treated the AKMT-knockout parasites with Jas and found that stabilization of the actin filaments recovered force generation in the mutant to the same level as in Jas-treated wild-type parasites, with a mean force of 3.5 ± 0.6 versus 3.7 ± 0.3 pN ($p = 0.4$) and a maximum force of 6.1 ± 0.3 versus 6.6 ± 0.7 pN ($p = 0.3$; Figure 7, KO-Jas; $n = 5$; Table 1). This suggests that force transmission occurs normally in mutant parasites but that force generation is impaired in the absence of AKMT. This could be due to a decrease in motor activity or a decrease in actin filament number or length. Although it is possible that stabilization of the actin filaments by Jas somehow compensates for a lack of motor activity (a decrease in the number of active motors or the duty cycle of the motor), it is difficult to envision how this compensation could restore force generation to exactly the wild-type level. We thus favor the hypothesis that AKMT is an upstream regulator of actin polymerization.

In contrast to the response to Jas, ionomycin treatment restored the ability of AKMT knockouts to polarize ($r = 0.57 \pm 0.01$). However, the mean magnitude of force generation was only partially recovered at 2.1 ± 0.5 pN ($n = 5$; KO-Iono, Figure 7) and remained significantly lower than that for ionomycin-treated wild-type parasite (4.8 ± 0.6 pN; Table 1). These data confirm that calcium signaling controls the polarization of the force and show that polarization does not require a high magnitude of force.

DISCUSSION

The actomyosin motile systems of Apicomplexa glideosomes are commonly illustrated and implicitly understood as illustrated in Figure 1C—as a one-dimensional arrangement of proteins already assembled parallel to the long axis of the cell. In contrast to this assumption, our data show that the glideosome is not fully preassembled with a polar orientation. Instead, *Toxoplasma* may assemble components of the glideosome in response to receptor ligation and/or calcium release, thus activating polar motility. Although some level of force is generated even from the earliest moments of receptor ligation, it is generated transiently and with little directional preference and is therefore incapable of driving directional motility. Thus the transition from apolar to polar force generation is a critical step in the life cycle of *Toxoplasma*.

Our data show that force generation and polarization are separable, although not necessarily separately regulated. During the apolar phase, the organism generates maximum forces in random

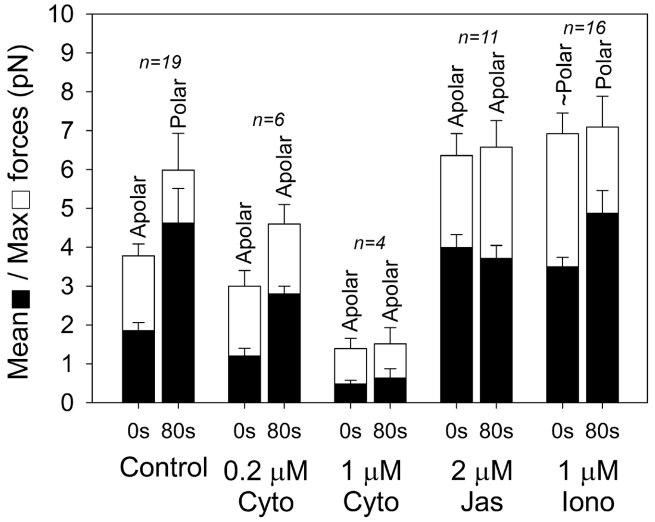

FIGURE 6: The mean (black) and maximum (white) apolar and polar forces for each experimental condition using wild-type parasites measured at the beginning (0 s) and end (80 s) of each experiment. The directionality of the force is shown as apolar (no fixed orientation), polar (a defined orientation), or ~polar (in transition). The error bars show SEM.

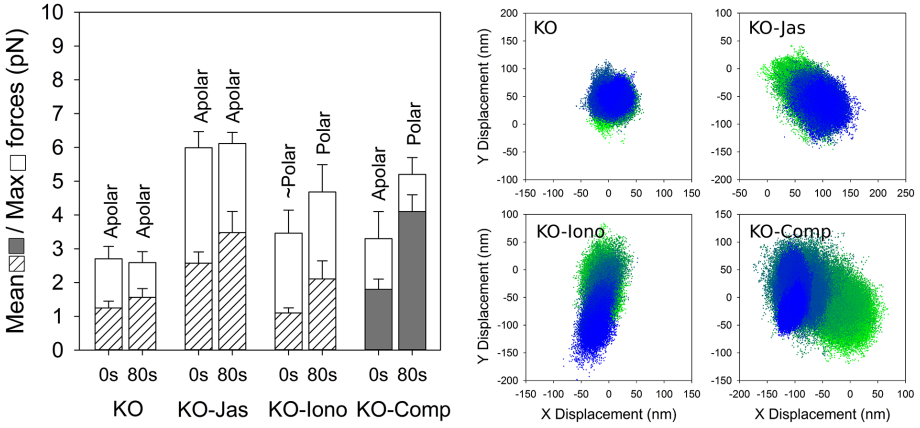

FIGURE 7: Knockout (KO) of a novel lysine methyltransferase (AKMT) inhibits the ability of *Toxoplasma* to polarize and generate force. This reduction in force is reversible by Jas (KO-Jas), and the ability to polarize but not the ability to generate force is reversible by ionomycin (KO-Iono). Wild-type force is restored in the complemented organism (KO-Comp). Mean force (hashed and gray) and maximum force (white) are both shown, along with example 2D displacement plots of each condition. In each graph, the data are color-coded by time, from green, representing 0 s, to blue, representing 80 s. The basal end of the parasite is toward the bottom of each 2D plot (negative in *y*). The error bars show SEM.

directions that are equal in magnitude to the highest sustained forces during the polar phase. In addition, our jasplakinolide data show that turnover of monomers from actin filaments is not necessary for motility per se but *is* necessary to achieve directional motility. Finally, polarity in AKMT-knockout parasites can be recovered by an increase in intracellular calcium concentration via ionomycin treatment, but with only partial restoration of force. Thus, force magnitude and force directionality are not intrinsically linked in this organism. An ability to vary the direction of force generation might be of benefit to these organisms for navigating through the dramatically different environments they experience during their complex life cycles.

The transition from the apolar to polar phase constitutes two stages: a sudden, lateral movement (jump), and the subsequent generation of force directed toward the basal end of the parasite. This transition occurs ~60 s after microsphere contact and is strictly dependent on the state of actin polymerization, as either inhibition of actin polymerization or uncontrolled promotion of actin polymerization abrogate the polar phase, as well as the lateral jump. Further, the kinetics of transition from the apolar to the polar phase is regulated by calcium. When treated with ionomycin, which elevates the intraparasite calcium concentration, the translocation of the microsphere is well aligned with the longitudinal axis of the parasite from the beginning of our measurements, indicating that components of the cortical motility apparatus are activated in a calcium-dependent manner.

The mean of the jump distance in wild-type untreated parasite is 139 ± 20 nm, close to half of the spatial interval (~286 nm) of the inner-membrane particles coaligned with the cortical microtubules, and thus it is conceivable that these rows of inner-membrane particles provide spatial constraints for aligning the motility apparatus. Note that under the unconstrained condition, the lateral jump was measured to be almost exactly twice that under the constrained condition (261 ± 53 vs. 139 ± 20 nm). We hypothesize that when constrained by the laser trap, the actin, receptors, and associated microsphere have no option but to be pulled onto the nearest track of myosin molecules. When unconstrained, Brownian motion of the assemblage may allow it the freedom to jump onto a more distant track.

Once polarity is established, the forces generated by the glideosome are fully compatible with cell motility. The estimated contact area surveyed by our 0.6-μm microspheres coupled through MIC2 to the membrane is ~0.04 μm^2. If the force acting on this area (~5 pN) is replicated across the entire surface area of the organism (~17 μm^2, estimated as a pair of conical surfaces), then the summed cortical force in a 3D tissue could be as high as ~2 nN. This is similar in whole-cell force to that measured in chemotactic pulmonary macrophages (2–5 nN) isolated from mice and hamsters (Guilford *et al.*, 1995), although these macrophages are significantly larger than *T. gondii.* From these values, we estimate a traction force of 125 Pa, similar to the traction forces in *P. berghei* sporozoites (~200 Pa) measured by traction force microscopy (Münter *et al.*, 2009). We also expect the localized adhesion forces between the parasite and the host cell to be of similar magnitude. Indeed, adhesive forces between *Plasmodium falciparum* merozoites and red blood cells have been measured at ~40 pN (Crick *et al.*, 2014). That study did not report a contact area between the two cells, although it would be larger than the contact area between the microsphere and the parasite measured here.

The main axis force measured here (3.3 pN) is equivalent in time-averaged stall force to around eight myosin heads (~0.4 pN/head, from measurements of 0.2–0.6 pN per myosin head; VanBuren *et al.*, 1995; Rao *et al.*, 2009). *T. gondii* actin, however, is believed to form filaments only ~100 nm in length (Dobrowolski *et al.*, 1997; Schmitz *et al.*, 2005; Sahoo *et al.*, 2006). Because myosin binding sites are arranged helically about the actin filament, when viewed from the perspective of myosin on the IMC, those binding sites will be accessible only every half-axial repeat of the filament structure, or 37 nm. This seemingly leaves room for only three myosin heads to bind and creates an obvious disconnect between the number of binding sites needed on an actin filament to account for the forces measured here and the number of binding sites thought available on actin filaments of that length. We envision three possible ways around this discrepancy. First, more than one actin filament might bind in parallel to a given microsphere contact point. Second, three MyoAs may be able to bind at each half-axial repeat; indeed, there is experimental evidence of myosin on a flat surface having access to "target zones" on actin that are three binding sites wide (Steffen *et al.*, 2001), although evidence is lacking of simultaneous binding of three myosins at each. Finally, it is possible that the in vivo lengths of apicomplexan actin filaments have been underestimated. Indeed, the maximum displacements measured here in the polar phase (202 ± 31 nm in control) might be a reasonable estimate of the minimum actin filament lengths in vivo; this would provide nearly enough binding sites to account for our data.

Although short filaments and rapid turnover of actin monomers are important to motility in Apicomplexa (Shaw and Tilney, 1999; Wetzel *et al.*, 2003; Skillman *et al.*, 2011), it is not known how the local force produced by myosin motor can be converted into directional movement spanning tens of micrometers because there are no structures analogous to dense plaques or z-disks to serve as polar anchors for microfilaments. Our data support a model (Figure 8) in which motility is limited by the availability of sufficiently

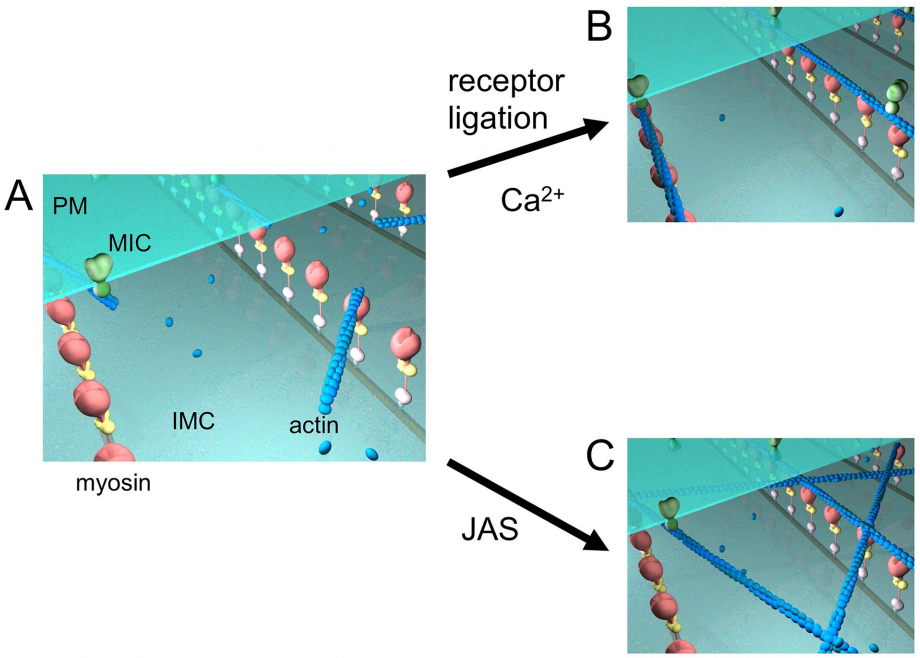

FIGURE 8: Revised model of glideosome function in *T. gondii*. (A) The glideosome may consist of orderly, directional arrays of myosin molecules anchored to the IMC. In its resting state, we propose that short actin filaments are randomly oriented across this array and therefore subject to randomly directed, transient forces from myosin. (B) Receptor ligation and/or increase in intracellular calcium causes an orderly elongation of the actin filaments, which become restricted to and polarized along the preexisting myosin tracks. Possible mechanisms for this polarization include directionally biased polymerization of the actin under the influence of myosin and mechanical alignment of actin filaments once they are elongated. (C) We propose that treatment with Jas causes rapid assembly of a randomly oriented actin filament mesh that cannot support directional motility, even though the absolute magnitude of force generation by myosin is largely unaffected.

long actin filaments to sustain force or motion. We envision the myosin motors being arranged along orderly, longitudinal tracks in the pellicle, ~230 nm apart laterally, and with the power stroke preferentially oriented toward the basal end of the cell. Indeed, there is evidence that myosin is well anchored within the IMC, even without the aid of cytoskeletal elements (Johnson *et al.*, 2007). When cell surface receptors are first ligated, the underlying, short actin filaments might engage along these longitudinal tracks or might swivel to engage across parallel tracks, resulting in a range of angles in force generation (apolar). A subsequent increase in intracellular calcium causes a slow polymerization of the actin filaments, which subsequently adopt the polarization of the underlying array of myosin motors. This would prove to be an unusual mechanism because actin filament polarity ordinarily dictates actin's direction of travel over a particular myosin. For this mechanism to work, one of two conditions would need to be satisfied. Either 1) myosin arrays would have to pull actin filaments preferentially into alignment with the minus ends toward the basal pole of the parasite, or 2) actin filaments would have to be preferentially polymerized along the tracks with the minus end toward the basal pole. There is in vitro evidence to support either of these mechanisms. For instance, micropatterned heavy meromyosin on lines restricts actin filaments to the lines (Kinosita *et al.*, 1993; Bunk *et al.*, 2003), supporting the mechanism that orderly rows of myosin pull actin filaments into polar alignment. On the other hand, myosin on a surface orients the polymerization of growing actin filaments (Interliggi *et al.*, 2007), supporting the mechanism that actin filaments are polymerized into polar alignment. In addition, single-headed myosins have been shown in yeast to serve as actin filament nucleators (Lechler *et al.*, 2000), raising the possibility that the single-headed MyoA motor can be regulated to induce polarized actin filament growth or cause properly aligned actin filaments to grow more quickly. Either mechanism would be sensitive to the rate of actin filament polymerization and orientation, as we found in our data. For example, we interpret our jasplakinolide data as the actin filaments growing too long and too quickly and therefore either 1) unable to orient to the long axis of the parasite or 2) not subject to preferential polymerization along the correct axis (Figure 8).

Another important question is whether actin filament polymerization is the only regulated parameter in this motile system. The near full recovery of alignment with only partial recovery of force in ionomycin-treated AKMT knockouts can be interpreted as there being a minimum actin filament length that must be reached in order to achieve polar alignment and that any growth beyond that length would simply allow more motors to engage on the filaments, increasing force. Alternatively, the data might be interpreted to mean that the myosin motor must be activated separately from actin filament polymerization. It is also interesting that the maximum force for untreated and Jas-treated parasites is similar (6.0 vs. 6.6 pN), which suggests that something other than the length and/or density of actin filaments is limiting force generation in the parasite.

Indeed, our observation of sustained forces, even low ones, during the polar phase is important and surprising because of the very low duty ratio measured for MyoA in vitro (0.8%; Heaslip *et al.*, 2010). With such a low duty ratio, only a few myosin motors could engage on an actin filament at any moment in time; several hundred motors would be required to ensure that at least one is bound to the actin filament at any given instant. If these duty cycle estimates are accurate, one should observe random rather than productive, continuous movement. This is consistent with our observations of low but highly variable force during an apolar phase but not with the sustained forces of the polar phase. It is therefore possible that the properties of MyoA measured in vitro will not be fully representative of its normal function. Mammalian actin has been used in in vitro motility assays out of necessity (Heaslip *et al.*, 2010) because apicomplexan actins cannot be polymerized to significant length in vitro. Yet it has been shown that MyoA binds to mammalian actin in a different way than do mammalian myosins (Herm-Gotz *et al.*, 2002). Further, surface-adsorbed motors in vitro may be partially denatured or missing protein–protein contacts (e.g., GAP45) that may be critical to function and thus alter the duty ratio.

These data underscore the need for measuring actin and myosin function in the in vivo environment. Although others have measured the function of purified myosin through motility assays and laser trap–microneedle transducers (Herm-Gotz *et al.*, 2002; Heaslip *et al.*, 2010), the experiments presented here are the first of their

kind to fully quantify the molecular forces involved in the motility behavior of Apicomplexa in the context of live parasites. It will be important also to compare these data with those collected from other apicomplexan genera because significant differences remain between them (Kim and Weiss, 2004). Despite their overall similarities, they may differ greatly in either the mechanobiology of their motile machinery or the direct regulation thereof. Finally, the measurements were made here under auxotonic conditions—the load on the microsphere changed proportionately as displacement of the microsphere changed. It will be important to characterize force generation by these organisms under the more rigorously defined isometric and isotonic conditions.

MATERIALS AND METHODS

Cell culture

T. gondii (RH strain), basal end–labeled *Toxoplasma* (enhanced green fluorescent protein [eGFP]–TgMORN1; Hu *et al.*, 2006; Hu, 2008), the AKMT-knockout parasite, and the FLAG-AKMT complemented line (Heaslip *et al.*, 2011) were maintained in vitro in serial cultures of human foreskin fibroblast (HFF) cell cultures. HFF cells were grown to confluence with a growth medium containing 10% heat-inactivated newborn calf serum, 1% Na pyruvate, and 1% L-glutamine in DMEM. Once inoculated, cultures were kept with a maintenance medium, in which the percentage of heat-inactivated newborn calf serum was reduced to 1%. To collect lysate, infected cultures were allowed to incubate until *Toxoplasma* tachyzoites had lysed ~50% of the host cells, and then the surface of the flask was scraped to bring parasites into suspension. Part of the lysate was used in the preparation of the flow cells needed for laser trapping. The remaining lysate was spun down in a centrifuge (1000 × g at 4°C for 14 min) and resuspended in freezing medium for storage in liquid nitrogen.

Laser trap

The laser trap system used for these experiments has been described elsewhere (Guilford *et al.*, 2004), but with modifications. The collimated beam of a fiber laser (25 W, 1090 nm; SPI Lasers SP-S-20-B-1090-A-30-UAC) was passed through a Glan laser prism and a half-wave plate before entering the aperture of a two-axis acoustooptic deflector (6 mm; NEOS). The primary diffracted beam was expanded through an afocal system of lenses (Fällman and Axner, 1997) to fill the back aperture of a microscope objective (Olympus UPLFL 1.3 numerical aperture/100×). Light exiting the flow cell was collected for back focal plane interferometry (Allersma *et al.*, 1998) exactly as described in Guilford *et al.* (2004). A field-programmable gate array (National Instruments PCI-7833R) controlled the acoustooptic deflector and collected data. The microscope stage was an nPoint NPXY150Z50C with subnanometer stability. A laser power of 1 W was used for these experiments (estimated 300 mW in the specimen plane), at which all organisms survived. Bright-field imaging was accomplished with a charge-coupled device (CCD; Pulnix), and imaging of GFP-expressing parasites was accomplished with an intensified CCD (IC-200; PTI). Except where otherwise stated, optics were from Newport Corporation.

Experimental approach

Flow cells of ~40 µl volume were prepared by stacking 18 × 18 mm coverslips on top of 22 × 22 mm coverslips, which were separated by Mylar shims (Laib *et al.*, 2009; Python *et al.*, 2010). These flow cells were injected with solutions of 10 mg/ml poly-L-lysine (30–70 kDa; P2636; Sigma-Aldrich) before loading of the parasite suspension. Parasites were allowed to settle onto the polylysine-coated surface of the flow cell for at least 20 min before flushing with medium to remove cell debris and nonadherent parasites. Nonfunctionalized silica microspheres (0.60 µm; Bangs Laboratories) were washed three times with water and suspended in the medium of interest—HFF Maintenance Medium, with or without 2 µM Jas (J4580; Sigma-Aldrich), 1 µM ionomycin (I9657; Sigma-Aldrich), or 200 nM or 1 µM cytochalasin D (C8273; Sigma-Aldrich). This suspension was loaded slowly into the flow cell. Once loaded, the flow cell was sealed at its ends with vacuum grease and placed on the laser trap stage.

Only organisms that were immobile and adhered lengthwise to the surface of the flow cell were used for experiments. The trap was used to capture free-floating microspheres in solution. Once captured, the single microsphere was positioned at a depth of 3 µm relative to the surface of the flow cell. The laser trap was rapidly displaced in a series of 200-nm steps along both the *x*- and *y*-axes for use in calibration. The microsphere was raised to ~5 µm, moved over the center of the parasite, and then lowered carefully onto the surface of the organism (Figure 1E).

For the unconstrained conditions, microsphere were imaged every 5 s from the moment of release to the moment the microsphere touched the substrate at the edge of the cell. Images were captured under bright-field imaging.

For constrained conditions, the microsphere was trapped on the surface of the cell for a period of 3 min, and data were collected at a sampling rate of 50 kHz. A micrograph was taken of each parasite for comparison with the direction of microsphere displacement. The laser trap data presented here include measurements from 4–19 parasites, depending on the experimental condition. To confirm that the movement of the microsphere was from the apical to the basal end during the polar phase, we repeated these measurements with *Toxoplasma* whose basal end was fluorescently labeled by eGFP-TgMORN1 a component of the basal complex (Figure 1D; Hu *et al.*, 2006; Hu, 2008). The data confirm that once in the polar phase, the force is always directed towards the basal end. The mean absolute force during the polar phase measured in these fluorescent parasites was the same as control (4.0 ± 0.3 pN, $n = 6$, $p = 0.2$). Further, force measured in vehicle-only (dimethyl sulfoxide) controls did not differ from that in untreated parasites ($p = 0.2$).

Data analysis for unconstrained conditions

The movements of unconstrained microspheres were tracked by cross-correlation of video frames using methods described in Cheezum *et al.* (2001). The jump distance was calculated manually by measuring the distance between the first measured coordinate after microsphere release and the data point immediately preceding retrograde transport of the microsphere.

Data analysis for constrained conditions

Data analysis was performed using proprietary software developed in Delphi (Borland). Each microsphere was calibrated before use along both *x*- and *y*-axes using both step response (Dupuis *et al.*, 1997) and power spectral density (Svoboda and Block, 1994). Typical trap stiffness values were 0.020 ± 0.001 and 0.025 ± 0.002 pN/nm along the *x*- and *y*-axes, respectively. Trap stiffness determined with the microsphere directly above the parasite did not differ significantly ($p = 0.46$) from results using our standard approach, which is to perform the stiffness and sensitivity calibrations several micrometers to the side of the parasite.

The start time of each trial was determined by examining the *z*-axis signal and establishing the point at which the microsphere made contact with the surface of the cell and no further movement

of the microscope stage was made. The baseline mean for each data channel was determined over the subsequent 50 ms. Data were discarded if there was appreciable motion of the microsphere along the *z*-axis once stage motion had ceased. The data were Gaussian filtered to 1 kHz after calibration but before analysis.

The measured forces and displacements in *x* and *y* were combined using the Pythagorean theorem to give a force magnitude. The duration of the apolar phase was measured from this force magnitude as the time difference between the start of the trial and either a sudden increase in mean force or a sudden decrease in the variance of the force. Maximum force magnitudes and maximum displacements were measured over the first 30 and final 20 s of each 80-s trial. Both of these measurements represent the data point with the maximum force and/or displacement relative to baseline during the specified time period. Mean force magnitudes were measured over the first and final 10 s of each trial.

The main-axis force vector was determined by fitting a line using Deming regression through data from the last 10 s of each 80-s trial. The "jump" distance (*J*) was determined by calculating the perpendicular distance between this line and the baseline mean established at parasite contact (as described earlier). To determine the polar force component (*P*) along this line, we calculated the mean projection of the *x* and *y* force components onto the main axis vector and then measured *P* as the distance of this mean projection from the intersection of the jump vector (*J*) and the main axis vector (Figure 3A).

Anisotropy was calculated as follows. For a given segment of data, we determined the best fit line by Deming regression. We subsequently determined the distance of every data point from that line and calculated RMS "perpendicular" displacement ($\perp$). We similarly determined the distance from the closest point on the line for each data point to the mean projection of the data onto the best-fit line. From these, we calculated RMS "parallel" displacement ($\parallel$). Anisotropy (r) was calculated as $r = (\parallel - \perp) / (\parallel + 2\perp)$. We measured anisotropy over the first 10 s and over the span of 70–80 s of each experimental trial. An anisotropy value of 0 indicates no directional preference, and an anisotropy value of 1 indicates that all the data fall directly on a straight line.

ACKNOWLEDGMENTS

We thank Jun Liu (Indiana University) for the superresolution image of parasites expressing mEmeraldFP-TrxL1 and mTagFP-TgMORN1. We thank Daniella Fuller for the inset micrograph in Figure 1. This work was supported by a grant from the National Institute of Allergy and Infectious Disease (R01AI098686 to K.H. and subcontract to W.H.G. and B.P.H.). This research was also supported in part by funding from the March of Dimes (6-FY12-258) to K.H., National Science Foundation Grant NSF PHY11-25915, and Gordon and Betty Moore Foundation Award 2919 to the Kavli Institute for Theoretical Physics of the University of California, Santa Barbara. We also acknowledge the generous support to R.V.S. of the University of Virginia, offices of the Dean of the School of Engineering, the Dean of the College of Arts and Sciences, and the Vice President for Research.

REFERENCES

Allersma MW, Gittes F, deCastro MJ, Stewart RJ, Schmidt CF (1998). Two-dimensional tracking of ncd motility by back focal plane interferometry. Biophys J 74, 1074–1085.

Andenmatten N, Egarter S, Jackson AJ, Jullien N, Herman J-P, Meissner M (2013). Conditional genome engineering in Toxoplasma gondii uncovers alternative invasion mechanisms. Nat Methods 10, 125–127.

Baum J, Richard D, Healer J, Rug M, Krnajski Z, Gilberger T-W, Green JL, Holder AA, Cowman AF (2006). A conserved molecular motor drives cell invasion and gliding motility across malaria life cycle stages and other apicomplexan parasites. J Biol Chem 281, 5197–5208.

Block SM, Asbury CL, Shaevitz JW, Lang MJ (2003). Probing the kinesin reaction cycle with a 2D optical force clamp. Proc Natl Acad Sci USA 100, 2351–2356.

Bunk R, Klinth J, Montelius L, Nicholls IA, Omling P, Tågerud S, Månsson A (2003). Actomyosin motility on nanostructured surfaces. Biochem Biophys Res Commun 301, 783–788.

Burney A, Lugton I (2009). Prevalence and Effect of Theileria Infection in NSW South Coast Cattle Herds: A Targeted Surveillance Study Financially Supported by NSW DII, Sydney, Australia: South East Livestock Health and Pest Authority.

Caldas LA, de Souza W, Attias M (2007). Calcium ionophore-induced egress of Toxoplasma gondii shortly after host cell invasion. Vet Parasitol 147, 210–220.

Caldas LA, de Souza W, Attias M (2010). Microscopic analysis of calcium ionophore activated egress of Toxoplasma gondii from the host cell. Vet Parasitol 167, 8–18.

Carruthers VB, Giddings OK, Sibley LD (1999). Secretion of micronemal proteins is associated with toxoplasma invasion of host cells. Cell Microbiol 1, 225–235.

Carruthers VB, Sibley LD (1999). Mobilization of intracellular calcium stimulates microneme discharge in Toxoplasma gondii. Mol Microbiol 31, 421–428.

Cheezum MK, Walker WF, Guilford WH (2001). Quantitative comparison of algorithms for tracking single fluorescent particles. Biophys J 81, 2378–2388.

Crick AJ, Theron M, Tiffert T, Lew VL, Cicuta P, Rayner JC (2014). Quantitation of malaria parasite-erythrocyte cell-cell interactions using optical tweezers. Biophys J 107, 846–853.

Dobrowolski JM, Niesman IR, Sibley LD (1997). Actin in the parasite Toxoplasma gondii is encoded by a single copy gene, ACT1 and exists primarily in a globular form. Cell Motil Cytoskeleton 37, 253–262.

Dobrowolski JM, Sibley LD (1996). Toxoplasma invasion of mammalian cells is powered by the actin cytoskeleton of the parasite. Cell 84, 933–939.

Dubey JP (2009). Toxoplasmosis in sheep—the last 20 years. Vet Parasitol 163, 1–14.

Dupuis DE, Guilford WH, Wu J, Warshaw DM (1997). Actin filament mechanics in the laser trap. J Muscle Res Cell Motil 18, 17–30.

Dzbenski TH, Michalak T, Plonka WS (1976). Electron microscopic and radioisotopic studies on cap formation in Toxoplasma gondii. Infect Immun 14, 1196–1201.

Fällman E, Axner O (1997). Design for fully steerable dual-trap optical tweezers. Appl Opt 36, 2107–2113.

Fornace KM, Clark EL, Macdonald SE, Namangala B, Karimuribo E, Awuni JA, Thieme O, Blake DP, Rushton J (2013). Occurrence of eimeria species parasites on small-scale commercial chicken farms in Africa and indication of economic profitability. PLoS One 8, e84254.

Gaskins E, Gilk S, DeVore N, Mann T, Ward G, Beckers C (2004). Identification of the membrane receptor of a class XIV myosin in Toxoplasma gondii. J Cell Biol 165, 383–393.

Gonzalez V, Combe A, David V, Malmquist NA, Delorme V, Leroy C, Blazquez S, Ménard R, Tardieux I (2009). Host cell entry by apicomplexa parasites requires actin polymerization in the host cell. Cell Host Microbe 5, 259–272.

Guilford WH, Lantz RC, Gore RW (1995). Locomotive forces produced by single leukocytes in vivo and in vitro. Am J Physiol 268, C1308–C1312.

Guilford WH, Tournas JA, Dascalu D, Watson DS (2004). Creating multiple time-shared laser traps with simultaneous displacement detection using digital signal processing hardware. Anal Biochem 326, 153–166.

Heaslip AT, Leung JM, Carey KL, Catti F, Warshaw DM, Westwood NJ, Ballif BA, Ward GE (2010). A small-molecule inhibitor of T. gondii motility induces the posttranslational modification of myosin light chain-1 and inhibits myosin motor activity. PLoS Pathog 6, e1000720.

Heaslip AT, Nishi M, Stein B, Hu K (2011). The motility of a human parasite, Toxoplasma gondii, is regulated by a novel lysine methyltransferase. PLoS Pathog 7, e1002201.

Herm-Gotz A, Weiss S, Stratmann R, Fujita-Becker S, Ruff C, Meyhofer E, Soldati T, Manstein DJ, Geeves MA, Soldati D (2002). Toxoplasma gondii myosin A and its light chain: A fast, single-headed, plus-end-directed motor. EMBO J 21, 2149–2158.

Hu K (2008). Organizational changes of the daughter basal complex during the parasite replication of Toxoplasma gondii. PLoS Pathog 4, e10.

Hu K, Johnson J, Florens L, Fraunholz M, Suravajjala S, DiLullo C, Yates J, Roos DS, Murray JM (2006). Cytoskeletal components of an invasion machine—the apical complex of Toxoplasma gondii. PLoS Pathog 2, e13.
Interliggi KA, Zeile WL, Ciftan-Hens SA, McGuire GE, Purich DL, Dickinson RB (2007). Guidance of actin filament elongation on filament-binding tracks. Langmuir 23, 11911–11916.
Johnson TM, Rajfur Z, Jacobson K, Beckers CJ (2007). Immobilization of the type XIV myosin complex in Toxoplasma gondii. Mol Biol Cell 18, 3039–3046.
Kijlstra A, Jongert E (2008). Control of the risk of human toxoplasmosis transmitted by meat. Int J Parasitol 38, 1359–1370.
Kim K, Weiss LM (2004). Toxoplasma gondii: the model apicomplexan. Int J Parasitol 34, 423–432.
King CA (1981). Cell surface interaction of the protozoan Gregarina with concanavalin A beads—implications for models of gregarine gliding. Cell Biol Int Rep 5, 297–305.
Kinosita K, Suzuki N, Ishiwata S, Nishizaka T, Itoh H, Hakozaki H, Marriott G, Miyata H (1993). Orientation of actin monomers in moving actin filaments. Adv Exp Med Biol 332, 321–328.
Laib J, Marin J, Bloodgood R, Guilford W (2009). The reciprocal coordination and mechanics of molecular motors in living cells. Proc Natl Acad Sci USA 106, 3190–3195.
Lechler T, Shevchenko A, Li R (2000). Direct involvement of yeast type I myosins in Cdc42-dependent actin polymerization. J Cell Biol 148, 363–373.
Liu J, He Y, Benmerzouga I, Sullivan WJ Jr, Morrissette NS, Murray JM, Hu K (2016). An ensemble of specifically targeted proteins stabilizes cortical microtubules in the human parasite *Toxoplasma gondii*. Mol Biol Cell 27, 549–571.
Meissner M, Schlüter D, Soldati D (2002). Role of Toxoplasma gondii myosin A in powering parasite gliding and host cell invasion. Science 298, 837–840.
Monteiro VG, de Melo EJ, Attias M, de Souza W (2001). Morphological changes during conoid extrusion in Toxoplasma gondii tachyzoites treated with calcium ionophore. J Struct Biol 136, 181–189.
Morrissette NS, Murray JM, Roos DS (1997). Subpellicular microtubules associate with an intramembranous particle lattice in the protozoan parasite Toxoplasma gondii. J Cell Sci 110, 35–42.
Münter S, Sabass B, Selhuber-Unkel C, Kudryashev M, Hegge S, Engel U, Spatz JP, Matuschewski K, Schwarz US, Frischknecht F (2009). Plasmodium sporozoite motility is modulated by the turnover of discrete adhesion sites. Cell Host Microbe 6, 551–562.
Nichols BA, Chiappino ML (1987). Cytoskeleton of Toxoplasma gondii. J Protozool 34, 217–226.
Nichols BA, O'Connor GR (1981). Penetration of mouse peritoneal macrophages by the protozoon Toxoplasma gondii. New evidence for active invasion and phagocytosis. Lab Invest 44, 324–335.
Opitz C, Soldati D (2002). "The glideosome": a dynamic complex powering gliding motion and host cell invasion by Toxoplasma gondii. Mol Microbiol 45, 597–604.
Pappas G, Roussos N, Falagas ME (2009). Toxoplasmosis snapshots: global status of Toxoplasma gondii seroprevalence and implications for pregnancy and congenital toxoplasmosis. Int J Parasitol 39, 1385–1394.
Python JL, Wilson KO, Snook JH, Guo B, Guilford WH (2010). The viscoelastic properties of microvilli are dependent upon the cell-surface molecule. Biochem Biophys Res Commun 397, 621–625.
Quadt KA, Streichfuss M, Moreau CA, Spatz JP, Frischknecht F (2016). Coupling of retrograde flow to force production during malaria parasite migration. ACS Nano 10, 2091–2102.
Rao VS, Marongelli EN, Guilford WH (2009). Phosphorylation of tropomyosin extends cooperative binding of myosin beyond a single regulatory unit. Cell Motil Cytoskeleton 66, 10–23.
Russell DG (1983). Host cell invasion by Apicomplexa: an expression of the parasite's contractile system? Parasitology 87, 199–209.
Russell DG, Sinden RE (1981). The role of the cytoskeleton in the motility of coccidian sporozoites. J Cell Sci 50, 345–359.
Sahoo N, Beatty W, Heuser J, Sept D, Sibley LD (2006). Unusual kinetic and structural properties control rapid assembly and turnover of actin in the parasite Toxoplasma gondii. Mol Biol Cell 17, 895–906.
Schmitz S, Grainger M, Howell S, Calder LJ, Gaeb M, Pinder JC, Holder AA, Veigel C (2005). Malaria parasite actin filaments are very short. J Mol Biol 349, 113–125.
Shaw MK, Tilney LG (1999). Induction of an acrosomal process in Toxoplasma gondii: visualization of actin filaments in a protozoan parasite. Proc Natl Acad Sci USA 96, 9095–9099.
Sibley LD, Andrews NW (2000). Cell invasion by un-palatable parasites. Traffic 1, 100–106.
Skillman KM, Diraviyam K, Khan A, Tang K, Sept D, Sibley LD (2011). Evolutionarily divergent, unstable filamentous actin is essential for gliding motility in apicomplexan parasites. PLoS Pathog 7, e1002280.
Soldati D, Meissner M (2004). Toxoplasma as a novel system for motility. Curr Opin Cell Biol 16, 32–40.
Speer CA, Wong RB, Blixt JA, Schenkel RH (1985). Capping of immune complexes by sporozoites of Eimeria tenella. J Parasitol 71, 33–42.
Steffen W, Smith D, Simmons R, Sleep J (2001). Mapping the actin filament with myosin. Proc Natl Acad Sci USA 98, 14949–14954.
Stewart MJ, Vanderberg JP (1991). Malaria sporozoites release circumsporozoite protein from their apical end and translocate it along their surface. J Protozool 38, 411–421.
Svoboda K, Block SM (1994). Biological applications of optical forces. Annu Rev Biophys Biomol Struct 23, 247–285.
Tenter AM, Heckeroth AR, Weiss LM (2000). Toxoplasma gondii: from animals to humans. Int J Parasitol 30, 1217–1258.
VanBuren P, Guilford WH, Kennedy G, Wu J, Warshaw DM (1995). Smooth muscle myosin: a high force-generating molecular motor. Biophys J 68, 256S–258S.
Wetzel DM, Chen LA, Ruiz FA, Moreno SNJ, Sibley LD (2004). Calcium-mediated protein secretion potentiates motility in Toxoplasma gondii. J Cell Sci 117, 5739–5748.
Wetzel DM, Håkansson S, Hu K, Roos D, Sibley LD (2003). Actin filament polymerization regulates gliding motility by apicomplexan parasites. Mol Biol Cell 14, 396–406.
Wong TC, Desser SS (1976). Fine structure of oocyst transformation and the sporozoites of Leucocytozoon dubreuili. J Protozool 23, 115–126.
World Health Organization (2012). World Malaria Report 2012, Available at www.who.int/malaria/publications/world_malaria_report_2012/en/ (accessed 24 February 2017).